Published in final edited form as:
Biomaterials. 2012 June ; 33(16): 4157–4165. doi:10.1016/j.biomaterials.2012.02.029.

Biophysical control of invasive tumor cell behavior by extracellular matrix microarchitecture

Shawn P. Carey, **Casey M. Kraning-Rush**, **Rebecca M. Williams**, and **Cynthia A. Reinhart-King**
Department of Biomedical Engineering, Cornell University, Ithaca, New York, 14853, USA

Abstract

Fibrillar collagen gels, which are used extensively *in vitro* to study tumor-microenvironment interactions, are composed of a cell-instructive network of interconnected fibers and pores whose organization is sensitive to polymerization conditions such as bulk concentration, pH, and temperature. Using confocal reflectance microscopy and image autocorrelation analysis to quantitatively assess gel microarchitecture, we show that additional polymerization parameters including culture media formulation and gel thickness significantly affect the dimensions and organization of fibers and pores in collagen gels. These findings enabled the development of a three-dimensional culture system in which cell-scale gel microarchitecture was decoupled from bulk gel collagen concentration. Interestingly, morphology and migration characteristics of embedded MDA-MB-231 cells were sensitive to gel microarchitecture independently of collagen gel concentration. Cells adopted a polarized, motile phenotype in gels with larger fibers and pores and a rounded or stellate, less motile phenotype in gels with small fibers and pores regardless of bulk gel density. Conversely, cell proliferation was sensitive to gel concentration but not microarchitecture. These results indicate that cell-scale gel microarchitecture may trump bulk-scale gel density in controlling specific cell behaviors, underscoring the biophysical role of gel microarchitecture in influencing cell behavior.

Keywords

Collagen; Microstructure; ECM (extracellular matrix); Cell morphology; Cell spreading; Confocal microscopy

1. Introduction

The tumor microenvironment exhibits intricate control over cancer progression by affecting the behavior of tumor cells both within the tumor mass as well as those that have invaded the surrounding stroma [1,2]. A critical component of this microenvironment is the extracellular matrix (ECM), which is a complex and dynamic biopolymer network that

Corresponding author: Cynthia A. Reinhart-King, 302 Weill Hall, 526 Campus Road, Ithaca, NY 14853, Tel: (607) 255-8491, Fax: (607) 255-7330, cak57@cornell.edu.

Conflict of Interest
The authors confirm that there are no known conflicts of interest associated with this publication and there has been no significant financial support for this work that could have influenced its outcome.

provides tumor cells with integrated biophysical and biochemical cues that influence cell survival and differentiation signaling [3], cell-cell interactions, cell mechanics, tissue homeostasis [4–6], and ultimately, clinical outcome [7,8]. Recently, there has been increasing interest in decoupling physical and chemical microenvironmental stimuli to determine their relative roles in cancer progression, and *in vitro* model systems of the tumor microenvironment have emerged as useful tools to study extracellular regulation of tumor cell behavior. While it is now widely accepted that physical ECM properties such as matrix stiffness are critical regulators of cell biology in two-dimensional (2D) *in vitro* environments [9–12], the tumor microenvironment exhibits three-dimensional (3D) complexity and physical cell-scale features that obscure the distinction between biochemical and physical regulators of cell behavior [13–15]. Therefore, to fully appreciate how the ECM physically contributes to cancer progression, it will be critical to study tumor cell behavior in biophysically- and biochemically-defined 3D *in vitro* model systems that recapitulate the *in vivo* microenvironment.

Extracellular matrix is a heterogeneous, fibrous biopolymer network with tissue-specific molecular composition, organization, and function [13,16]. Notably, unlike ECM in 2D experimental systems, ECM in interstitial tissues exhibits three-dimensional cell-scale *microarchitecture* that is dependent primarily upon the dimensions and arrangement of the type I collagen structural fibers that comprise the matrix [17]. These collagen fibers can serve as adhesion substrates, steric barriers, and tracks, making them potent extracellular determinants of biophysical cell behavior [18–22]. Further, this collagen fiber network serves as both a transducer of exogenous forces and a source of endogenous micro-scale mechanical properties [23–25], and there is a growing body of experimental and theoretical work investigating the relationship among microarchitecture-derived cell-scale matrix mechanics, cellular biomechanics, and bulk mechanical properties [26–29]. Thus, since matrix microarchitecture is one of the most influential physically-instructive components of the ECM, it is an ideal candidate for *in vitro* studies of biophysical regulation of cell behavior.

A number of strategies have been employed to study biophysical cell behavior as a function of matrix microarchitecture. Generally, cells are seeded within 3D matrices composed of various biomaterials including type I collagen, fibrin, basement membrane extract, or cell-derived matrix [30,31] and the ECM and cells are visualized with confocal or multiphoton microscopy [16]. Several groups have controlled 3D matrix microarchitecture and mechanical properties in these systems by tuning the density of collagen I or Matrigel, consistently finding that increased polymer concentrations yield gels with higher moduli, decreased pore size, and increased steric barriers. Interestingly, these studies have shown that cell mechanobiology and matrix remodeling [32,33], morphogenesis [3,6], and cell migration [34–36] are dependent upon these steric and mechanical properties of the 3D ECM as controlled by bulk gel concentration. To more accurately recapitulate tissue-specific ECMs, several researchers have monitored cell behavior in composite ECMs created by supplementing collagen scaffolds with additional ECM proteins such as fibronectin and laminin [18,34], glycosaminoglycans (GAGs) such as hyaluronan and chondroitin sulfate [37], and the polysaccharide agarose [38]. While all of the above strategies changed the matrix microarchitecture and biophysical properties, these modifications also significantly altered the biochemical composition and bioactivity of the scaffolds, preventing the complete decoupling of physical and chemical microenvironmental stimuli.

To isolate ECM biophysics and biochemistry, several groups have developed strategies to tune the microarchitecture of pure type I collagen gels independently of bulk gel density and chemical modification. Collagen gel polymerization is initiated *in vitro* by raising an acidic solution of collagen to neutral pH, which causes soluble collagen to condense and crosslink

laterally into fibrils that subsequently elongate to form an entangled meshwork of fibers. Fiber density, and thus, matrix microarchitecture, depend upon the rate of this fibril self-assembly, which is influenced by parameters such as pH, temperature, and ionic strength [13,16]. Importantly, collagen assembly is rapid at low or very high ionic strength [39], high pH [24], and high temperature conditions [26,40], yielding gels with small pores and high fiber density. Conversely, assembly is slower under moderate ionic strength, low pH, and low temperature conditions, resulting in gels with relatively larger pores and sparse, but larger fibers. Recently, Yang, et al. assessed glioma cell behavior within pure collagen gels polymerized at high (small pores) and low (large pores) temperatures, and found that pore size positively regulated invasive migration [40]. While such studies have begun to characterize exclusively biophysical determinants of cell behavior, the precise roles of matrix microarchitecture are not yet fully understood.

In this study, two critical parameters – gel thickness and media type – were explored as polymerization parameters used to alter gel microarchitecture independently of gel concentration, pH, temperature, and ionic strength. Gel microarchitecture was assessed with confocal reflectance microscopy (CRM) and quantified with spatial autocorrelation methods. Findings from acellular experiments were exploited to create a culture system that was used to probe the relative influences of cell-scale gel microarchitecture and bulk gel concentration on the migratory, morphological, proliferative, and ECM remodeling behavior of embedded MDA-MB-231 highly metastatic breast adenocarcinoma cells.

2. Materials and Methods

2.1 Cell culture

GFP-expressing MDA-MB-231 highly metastatic breast adenocarcinoma cells (Cell BioLabs, San Diego, CA) were cultured at 37°C and 5% CO_2 in Dulbecco's Modified Eagle Medium (DMEM; Invitrogen, Carlsbad, CA) supplemented with 2 mM L-glutamine, 10% Fetal Bovine Serum (Atlanta Biologicals, Norcross, GA), 0.1mM MEM Non-Essential Amino Acids, and 1% penicillin-streptomycin (Invitrogen).

2.2 Collagen gel preparation

Type I collagen was extracted from rat tail tendons (Pel-Freez Biologicals, Rogers, AR) via acid-solubilization, purified via centrifugation and lyophilization, and reconstituted in 0.1% acetic acid at 10 mg/mL. For acellular gel microarchitecture experiments, 10 mg/mL stock collagen solution was diluted to the desired final concentration by gently mixing with culture media or PBS on ice and neutralized to pH 7.0 with 1N NaOH. Gel solution was seeded into glass-bottom 24-well plates (MatTek, Ashland, MA). To determine the effects of media formulation on collagen gel microarchitecture, several base media types were used to dilute collagen: Dulbecco's Modified Eagle Medium (DMEM), Minimum Essential Medium (MEM), (RPMI), Medium 199 (M199), and PBS (Invitrogen). To control gel thickness, either 250 μL or 1000 μL of neutralized gel solution was pipetted onto the glass bottom of 24-well plate. These volumes resulted in 'thin gels' (~1.5 mm thickness) and 'thick gels' (~5.3 mm thickness), respectively. Gels were incubated at 37°C for 60 minutes for collagen polymerization after which they were overlaid with additional pre-warmed culture media or PBS.

To mitigate the biochemical effects of media composition on cell behavior, all cell experiments were performed in collagen gels made with complete DMEM as described above. After stock collagen solution was diluted to either 1.5 mg/mL or 3.0 mg/mL with ice-cold DMEM, the solution was neutralized with NaOH and a small volume (<5% total gel volume) of MDA-MB-231/GFP cell suspension was added such that gels would contain 5 ×

10^4 cells/mL. As in acellular experiments, gel solutions were seeded into glass-bottom 24-well plates in 250 μL and 1000 μL volumes for 'thin gels' and 'thick gels', respectively. Gels were incubated at 37°C for 60 minutes for collagen polymerization after which they were overlaid with pre-warmed complete DMEM and cultured for 24 hours prior to time-lapse imaging and 48 hours prior to morphology measurements.

2.3 Quantitative characterization of collagen microarchitecture

Collagen gel microarchitecture was assessed with a Zeiss LSM700 confocal microscope on a Zeiss AxioObserver Z1 inverted stand equipped with a long working distance water-immersion C-Apochromat 40×/1.1 NA Zeiss objective and operated by ZEN software (v. 2010, Carl Zeiss MicroImaging GmbH, Jena, Germany). For confocal reflectance microscopy, a solid state 405 nm laser illuminated the gel and backscattered light from collagen fibers was captured through a 32-μm pinhole, giving 1-μm thick confocal slices. Pixel dwell time was 2.55 μs and four scans were averaged per image. All gel microarchitecture imaging was performed near the gel center approximately 200 μm above the glass with imaging parameters kept consistent to enable quantitative comparison of gel microarchitecture across treatments.

The dimensions of collagen gel fibers and pores were quantified from CRM images using ImageJ (v. 1.43u, National Institute of Health, Bethesda, MD). Briefly, ImageJ's grid feature was used to overlay horizontal lines spaced 15 μm apart over CRM images. The line-drawing feature was used to measure the length of all collagen fibers that intersected these horizontal guide lines (n ≥ 300 fibers/image). Pore diameter was measured as the horizontal distance between fibers intersecting the guide lines (n ≥ 200 pores/image). The single-image distributions and averages of fiber length (L_{Fiber}) and pore diameter (D_{Pore}) were analyzed for n = 4 images per gel condition from two independent experiments.

Two-dimensional spatial autocorrelations were used to automatically analyze CRM images of acellular collagen gels. This technique has been used to analyze alignment of image features [41], as well as to describe the characteristic dimensions of image features in relatively isotropic images [24,42], making it ideal for quantifying the microarchitecture of the gels in this study, which consist of randomly-aligned fibers. A custom-written algorithm was used in the IDL data analysis environment (Exelis Visual Information Solutions, Boulder, CO) to calculate the two-dimensional autocorrelation function (ACF) of mean-normalized CRM images of collagen gels:

$$ACF(\alpha,\beta)=\frac{(1/MN)\sum_{x=1}^{M}\sum_{y=1}^{N} i(x,y)i(x+\alpha,y+\beta)}{\left[(1/MN)\sum_{x=1}^{M}\sum_{y=1}^{N} i(x,y)\right]^2}-1,$$

where *i(x,y)* is the function representing an M × N pixel image, and α and β are the tessellation coordinates along the x and y axes, respectively. The resulting ACFs were fit to Gaussian surfaces and the $1/e^2$ half-width was defined as ω_{ACF}. Mean ω_{ACF} was interpreted as the characteristic collagen fiber dimension for n = 4 images per acellular gel condition from two independent experiments.

2.4 Analysis of cell behavior

Tumor cell behavior within thin and thick 1.5 mg/mL and 3.0 mg/mL gels collagen gels was monitored by time-lapse confocal fluorescence imaging with a Yokogawa CSU-X1 spinning disk confocal on a Zeiss AxioObserver Z1 inverted stand that was equipped with a Plan-Apochromat 10×/0.45 NA Ph1 Zeiss objective, Hamamatsu ORCA-ER camera, and a

temperature-, humidity-, and CO_2-controlled microscope incubation chamber. Cells were imaged at 15-minute intervals for 20 hours using AxioVision software (v. 4.8, Carl Zeiss MicroImaging GmbH, Jena, Germany). At each time point, 11 sequential focal planes were acquired in 10-μm z-steps at 5–10 positions near the gel center approximately 200 μm above the glass. Projected z-stacks were used for assessment of cell morphology, migration, and mitosis, with 5–15 isolated cells distinguishable per field of view. Cell morphology was examined from z-projections acquired 48 h after cells were seeded in collagen gels. Using ImageJ, isolated cells were outlined and the cell morphology parameters circularity and aspect ratio were measured for $n \geq 75$ cells per condition from three independent experiments. Circularity describes the roundness of a cell, and is defined as ($4\pi \times$ Area/Perimeter^2). Aspect ratio describes a cell's elongation, and is defined as (Major axis/Minor axis) of the best-fit ellipse for a cell.

For cell motility analysis, four-dimensional confocal fluorescence datasets were projected in both the time- and z-dimensions to create 2D fluorescence images that represented cells' entire migration history through the 20 h experiment. Cell motility index was measured as the ratio of a cell's time-projected area to its initial area for $n \geq 30$ cells per condition from three independent experiments. To account for a variety of motile phenotypes, all cells in the field of view were analyzed as long as they did not interact with other cells or divide during the experiment. To control and account for cell division, complete culture media was replaced immediately prior to time-lapse experiments and cell proliferation rate was quantified from time-lapse videos as the ratio of cell divisions to the initial number of cells in the field of view for $n \geq 15$ fields of view per condition from three independent experiments.

2.5 Statistical analysis

Data was compared by two-way analysis of variance (ANOVA) with post-hoc Tukey HSD tests using JMP Pro software (v. 9.0.2, SAS Institute, Cary, NC). Collagen gel microarchitecture measurements including fiber length, pore diameter, and ω_{ACF} were compared across five media formulations and two gel thicknesses for Fig. 3 and across two collagen concentrations and two gel thicknesses for Fig. 4. Cell behavior parameters including circularity, aspect ratio, motility index, and cell mitosis were compared across two collagen concentrations and two gel thicknesses. All data is reported as mean ± SE; statistical significance was considered with $p < 0.05$.

3. Results

3.1 Confocal reflectance microscopy of thickness- and media-type dependent collagen gel microarchitecture

Collagen gels are comprised of interconnected networks of micron-scale fibers and pores whose properties are largely determined during gel polymerization. Since fibers reflect focused laser light due to refractive index mismatch at interfaces between fibers and aqueous pores, confocal reflectance microscopy (CRM) is useful for nondestructively visualizing the microarchitecture of collagen gels. Here, CRM was used to probe this microarchitecture in 1.5 mg/mL collagen gels made with different media types and in two thicknesses. The CRM images in Fig. 1 show qualitatively dissimilar fiber and pore organization between thin (top) and thick (bottom) gels. Generally, thin gels consisted of a tight meshwork of short fibers while thick gels contained larger and more irregular pores as well as longer and more bundled fibers as compared to their thin counterparts for all media formulations studied. Further, while thin gels appeared more homogeneous and showed little variation among media formulations, thick gels were highly heterogeneous and showed increased variance among media types.

3.2 Quantitative assessment of collagen gel microarchitecture

To quantitatively compare ECM microarchitecture across treatment groups, CRM images of collagen gels were analyzed by measurement of fiber and pore dimensions as well as by automated spatial autocorrelation. Figure 2A shows representative images for thin (top) and thick (bottom) 1.5 mg/mL gels made with MEM. These images were used to calculate the 2D autocorrelation functions shown in Figure 2B. Since the ACF can be approximated by a 2D Gaussian surface, the $1/e^2$ radius was extracted and is shown as the red outline in Fig. 2B. The mean $1/e^2$ radii, or the mean ω_{ACF} lengths, were 2.0 μm and 5.8 μm for the thin and thick gels, respectively. Figure 2C shows frequency distributions of fiber lengths and pore diameters for the thin and thick gels in Fig. 2A. Mean fiber length, L_{Fiber}, was 4.6 μm and 8.6 μm and mean pore diameter, D_{Pore}, was 2.6 μm and 4.0 μm for the thin and thick gels in Fig. 2A, respectively. To determine the effects of media formulation and gel thickness on collagen gel microarchitecture, the analyses illustrated in Fig. 2B-D were applied to CRM images of collagen gels for each condition and mean L_{Fiber}, and D_{Pore}, and ω_{ACF} were averaged for n = 4 gels per condition from two independent experiments. Increased gel thickness induced an approximately two-fold increase in mean collagen fiber length across all media types (Fig. 3A). Average pore diameters were approximately 50% larger in thick gels than in thin gels for all media types (Fig. 3B). Similarly, the ω_{ACF} characteristic lengths calculated from automated autocorrelation analysis were larger in thick gels than in thin gels for all media types (Fig. 3C). For each parameter, a statistically significant difference was observed between media-matched thin and thick gels by two-way ANOVA.

While gel thickness significantly affected each of the three measured collagen gel microarchitecture parameters, media type alone did not induce any statistically significant change in pore diameter within thickness groups (Fig. 3B; statistics not shown in figure). However, both fiber length (Fig. 3A) and autocorrelation characteristic length (Fig. 3C) were sensitive to gel thickness as well as media type. For example, within the thick gel group, there was a statistically significant difference in mean fiber length and ω_{ACF} between gels made with DMEM and gels made with RPMI, M199, and PBS for thin and thick gels (statistics not shown).

Mean ω_{ACF} characteristic length correlated well with mean fiber length for all conditions when assessed on a per-image basis ($R^2 = 0.88$) as both ω_{ACF} and fiber length showed comparable ranges of values for all gel images analyzed. However, ω_{ACF} correlated less strongly with pore diameter ($R^2 = 0.47$) as the latter exhibited a biphasic thickness-dependent, media type-independent response (Fig. 3D). However, the analyses in Fig. 3D could be used to differentiate gels by thickness, with gels clustered on the left (thin gels) and right (thick gels) of the dashed vertical lines.

3.3 Behavior of tumor cells within collagen gels

To investigate the effect of collagen gel microarchitecture on tumor cell behavior, GFP-expressing MDA-MB-231 cells were sparsely seeded into collagen gels and were monitored by confocal microscopy. To control for biochemical effects of media composition on cell behavior, only gels made with complete DMEM were used. To mitigate non-microarchitecture-related effects of gel thickness and probe the relationship between collagen gel concentration and microstructure, thin and thick 1.5 mg/mL gels as well as thin and thick high concentration 3.0 mg/mL gels were used. Confocal reflectance microscopy of cell-free areas of gels showed that both thin and thick 3.0 mg/mL gels resemble thin 1.5 mg/mL gels, with short collagen fibers organized into tight lattices, while thick 1.5 mg/mL gels contain larger pores and longer fibers (Fig. 4A, pore structures are highlighted with yellow dashed lines). Statistically significant increases in mean L_{Fiber}, and D_{Pore}, and ω_{ACF} were

observed for thick 1.5 mg/mL gels compared to all other gel conditions by two-way ANOVA (Fig. 4B).

3.3.1 Cell morphology—Because gel microarchitecture was consistent between thin and thick 3.0 mg/mL gels, these gels were used as controls for macro-scale effects of gel thickness such as nutrient availability and diffusion. Thus, using these gels together with thin and thick 1.5 mg/mL gels, cell behavior in response to micro-scale physical ECM traits could be studied in relative isolation. MDA-MB-231/GFP cells were cultured within collagen gels for 48 h. To capture population diversity in cell morphology, all single cells were analyzed in each z-projected field of view for each gel condition. Circularity describes the roundness of a cell and ranged from 0 to 1, with 1 denoting cells with rounded morphologies. Aspect ratio describes the elongation of a cell and was larger than 1, with increasing values denoting cells with increasingly polarized morphologies. These parameters were used together to describe the observed cell morphologies, which were distributed between two general morphology categories: 1) rounded, with high circularity and low aspect ratio (Fig. 5C, panels iii-iv), and 2) bipolar (elongated), with low circularity and high aspect ratio (Fig. 5C, panels i-ii). The distributions of cell morphologies observed in thin 1.5 mg/mL gels, thin 3.0 mg/mL gels, and thick 3.0 mg/mL gels were similar (Fig. 5). Further, cells embedded within these gels exhibited similar mean circularities and aspect ratios (Fig. 5, insets; no statistically significant differences among treatment groups were detected for either metric by two-way ANOVA). These generally low aspect ratios and mid-to-high circularities are consistent with rounded to multipolar morphologies (Fig. 5C, panels iii-iv). In contrast, cells in thick 1.5 mg/mL gels showed low circularities and an approximately two-fold enhancement in aspect ratio (Fig. 5A), consistent with increased bipolar cell spreading (Fig. 5C, panels i-ii). Mean circularity and aspect ratio for cells in these gels were significantly different from morphology parameters of cells in all other gel conditions (Fig. 5, insets). Notably, because of the relationship between aspect ratio and circularity, it was impossible for a cell to have both high aspect ratio and high circularity, resulting in the asymptotic distribution of morphologies (Fig. 5).

3.3.2 Cell motility—Since cell morphology and migration are closely interrelated biophysical cell behaviors, spontaneous random migration of cells embedded within collagen gels was monitored for 20 hours with time-lapse confocal microscopy. Representative confocal z-projections of an isolated MDA-MB-231/GFP cell migrating through collagen extracellular matrix at 0 h, 5 h, 10 h, and 20 h show that motile cell behavior consists of both random cell protrusions and cell body translation, both of which contribute to the 20-hour fluorescent “trail” of a migrating cell (Fig. 6A). Motility index was calculated as the ratio of a cell’s time- and z-projected area, A_{Sum}, (Fig. 6A, bottom panel) to its initial area, A_i (Fig. 6A, top panel). Cells in thin 1.5 mg/mL gels and thin and thick 3.0 mg/mL gels extended many protrusions (data not shown), but they did not exhibit substantial cell body translation, resulting in relatively low motility indices (Fig. 6B; no statistically significant differences among treatment groups). Conversely, cells in thick 1.5 mg/mL gels were both protrusive and highly motile, which contributed to a statistically significant two-fold increase in motility index for cells in these gels over the other three gel conditions (Fig. 6B). To ensure that gel microarchitecture-dependent differences in cell migration were independent of cell proliferation, only isolated cells that did not divide during the 20-hour analysis were analyzed.

3.3.3 Cell proliferation—To further characterize the effect of 3D collagen gel microarchitecture on cell behavior, cell proliferation rate was quantified from time-lapse datasets. While gel thickness did not affect the frequency of cell division, gel concentration induced a statistically significant difference in cell proliferation rate, with 3.0 mg/mL gels

showing an approximately 50% increase in cell proliferation frequency over 1.5 mg/mL gels (Fig. 6C).

4. Discussion

Collagen I hydrogels are widely used as *in vitro* ECM models to study tumor cell behavior in three-dimensional microenvironments because they possess biophysical and biochemical properties that can be tuned to match those of the interstitial tissues into which tumor cells invade [16]. Recently, there has been intense interest in determining how ECM properties such as stiffness, fiber alignment, and porosity regulate cell phenotype and can influence invasive tumor behavior [3,6,34,36,37,43–46]. However, despite these physical properties being tied to matrix microarchitecture [16,24,25,28], it remains to be determined how ECM microarchitecture alone can impact tumor cell biology. Here, collagen matrix structure was controlled independently of gel concentration by modulating gel thickness. Notably, preliminary studies with metastatic breast cancer cells show that tumor cell behaviors including morphology and migration can be regulated in a strictly microarchitecture-dependent manner.

4.1 Collagen gel microarchitecture is sensitive to gel thickness and media composition

In this study, low concentration 1.5 mg/mL collagen gels exhibited gel thickness-dependent differences in microarchitecture: thin gels (~1.5 mm thickness) were composed of tight networks of short, regular fibers while thick gels (~5.3 mm thickness) contained looser, more irregular networks consisting of longer and more substantially bundled fibers (Fig. 1). Quantitative image analysis showed that both thin and thick gels contained collagen fibers between 0 – 10 μm in length (Fig. 2C) and pores between 0 – 5 μm in diameter (Fig. 2D), but only thick gels contained fibers and pores with dimensions exceeding these ranges, resulting in statistically significant differences in mean fiber length (Fig. 3A), pore diameter (Fig. 3B), and, thus, the ω_{ACF} characteristic length (Fig. 3C) between thin and thick media type-matched gel replicates. Notably, the results of this study were consistent with previous reports showing that the rate of collagen fibril self-assembly and thus, fiber dimensions and organization, can be influenced by polymerization temperature [26,40] and/or treatment with pepsin, which removes cross-link mediating telopeptides [16]. As expected, thin collagen gels exhibited fiber and pore structures similar to those of gels rapidly polymerized at 37°C, while thick gels contained structural features analogous to gels polymerized slowly at 4–24°C [26]. Indeed, once 4°C gel solution was transferred to the culture plate and moved to 37°C, thin gels polymerized faster than thick gels (data not shown), presumably due to limited heat transfer in thick gels. The rapid increase in solution temperature in thin gels caused collagen monomers to quickly assemble, resulting in many polymer nucleation sites and thus, small pores and short fibers. Conversely, the relatively slow increase in collagen solution temperature in thick gels caused an impeded assembly phase, resulting in greater interfibrillar spacing, longer and thicker fibers, and increased heterogeneity.

While media type alone elicited statistically significant differences in fiber length and ω_{ACF} among some gel formulations (DMEM versus RPMI, M199, and PBS, for example), it did not significantly affect pore diameter within thickness groups (statistics among media types not shown in Fig. 3 for clarity). These results suggest that the temperature-dependent effects of gel thickness largely determine interfibrillar spacing and gel porosity, and that media composition, through ionic strength and/or the presence of other compounds during gelation [39], can affect fiber dimensions following assembly initiation. Given the variability in collagen fiber dimensions and ω_{ACF} among gels made with different base media types, these results demonstrate how sensitive the micro-scale structural features of collagen matrices are to polymerization conditions, and highlight the importance of monitoring gel microarchitecture in 3D ECM model systems.

Previously, Raub, et al. demonstrated the utility of two-dimensional spatial image correlation spectroscopy for measuring the characteristic dimensions of isotropic distributions of collagen fibers and matrix pores [24]. The authors modulated polymerization pH to tune gel microarchitecture and found that the image autocorrelation length parameter could be used to differentiate among matrix structures. In this study, mean ω_{ACF} showed a strong dependence on gel thickness, with thick gels exhibiting an approximately two-fold increase in characteristic length over their thin counterparts (Fig. 3C). Since ω_{ACF} is based upon image feature dimensions, it was expected that each image's ω_{ACF} would scale with its mean fiber length ($R^2 = 0.88$; Fig. 3D, left). The relatively poor correlation between ω_{ACF} and pore diameter ($R^2 = 0.47$; Fig. 3D, right) was also expected since pore size showed little dependence upon media type. These results support image correlation spectroscopy as an effective technique by which to automatically probe gel microarchitecture and differentiate between gel thickness-dependent matrix structure (Fig. 3D, dashed lines). Notably, the relatively small variability in mean fiber, pore, and ω_{ACF} measurements within treatment groups suggests that these metrics together comprise a suitable microarchitectural analysis scheme that could be employed to ensure gel consistency and validate experimental design of 3D collagen microenvironments for *in vitro* studies.

The finding that 3.0 mg/mL gels did not exhibit thickness-dependent microarchitecture is supported by previous work showing that higher concentration collagen gels polymerize more rapidly due to increased monomer availability [29]. The polymerization of high concentration gels was apparently insensitive to the subtle temperature differences in the gel thickness model, making thick and thin 3.0 mg/mL gels effective controls for non-microarchitecture related effects of gel thickness such as diffusion. Further, the structural resemblance of thin and thick 3.0 mg/mL gels to thin 1.5 mg/mL gels – small pores and small, regular fibers – allowed gel microarchitecture to be decoupled from bulk gel concentration in cell experiments such that *only* thick 1.5 mg/mL gels contained pores larger than 5 μm in diameter and long, sparse fibers (Fig. 4).

4.2 Microarchitectural control of tumor cell behavior

Recently, the role of the three-dimensional physical microenvironment in influencing cell behaviors such as adhesion, morphology, matrix remodeling, and migration has become a topic of intense interest as molecular mechanisms of 3D mechanotransduction – and 3D cell behavior in general – are increasingly understood [13,16,47,48]. Biophysical regulation of cell behavior has garnered particular interest in the cancer mechanobiology community due to tumor-associated changes in ECM structure and mechanics [16,44,45]. In this study, matrix microarchitecture was controlled independently of bulk gel concentration using a novel model system to investigate how this critical, yet understudied, ECM parameter can impact the behavior of embedded metastatic MDA-MB-231/GFP cells. Quantitative morphology analysis showed that thick 1.5 mg/mL gels (loose matrices) were substantially more permissive to bipolar cell spreading than thin 1.5 mg/mL gels and all 3.0 mg/mL gels (dense matrices). These findings are consistent with previous work with fibroblasts showing that cells within low concentration collagen gels exhibit more elongated morphologies than those within high concentration gels [32]. Notably, while all gels in this study contained cells with rounded and multipolar morphologies (Fig. 5C, panels iii-iv), only loosely networked gels contained an additional subpopulation of polarized cells (Fig. 5C, panels i-ii). These results suggest that structural properties of 3D ECM such as fiber and pore size can selectively facilitate bipolar, uniaxial cell spreading, which may enable other biophysical cell behaviors that are closely linked to morphology, such as migration [49–51].

Time-lapse microscopy revealed that the random migration of MDA-MB-231/GFP cells within collagen gels was sensitive to gel microarchitecture, with loose ECM (thick 1.5 mg/mL gels) more permissive to migration than dense ECM (Fig. 6B). While this study is the

first to demonstrate that collagen gel thickness-dependent matrix microarchitecture can regulate cell migration, these findings are consistent with previous reports that cell migration is more efficient within gels with larger pores [18,37,40,46]. In the present study, all gels contained pores that were 1–5 μm in diameter (Fig. 4A), but enhanced cell migration was observed only in thick 1.5 mg/mL gels, which contained pores with diameters greater than 5 μm (Figs. 4A and 6B). This apparent pore size threshold may be linked to nuclear deformability since pores larger than 5 μm would provide minimal steric resistance to the cell nucleus, which can be 5–15 μm in diameter in 3D microenvironments [52]. Interestingly, while cells in small-pore gels exhibited limited cell body translation, these cells continuously extended and retracted random pseudopodial protrusions (data not shown), suggesting that, even in a biophysically-restrictive 3D matrix, cells were still actively probing their microenvironment [53]. Together, these results imply that collagen gel thickness-dependent matrix microarchitecture regulates the three-dimensional migration of MDA-MB-231 cells through steric hindrance at matrix pores. Further analysis of behaviors such as matrix adhesion [3,32], remodeling [32,33,48], and degradation [46,54], all of which are sensitive to bulk matrix density, may provide additional insight into specific molecular mechanisms underlying the microarchitecture-dependent cell behaviors reported here.

A critical finding of this study is that bulk gel density does not necessarily reflect the cell-scale matrix density that cells perceive. By modulating gel thickness, it is possible to create low-density collagen gels that physically resemble high-density gels at the cellular scale. Interestingly, while microscale gel structure significantly affected cell morphology and migration regardless of gel concentration, cell proliferation was concentration-dependent, with cells cultured in 3.0 mg/mL gels exhibiting a significant increase in proliferation rate over those cultured in 1.5 mg/mL gels (Fig. 6C). Consistent with this finding, it has been shown that increased matrix density enhances proliferation in 3D due to an increase in matrix stiffness that accompanies increased density [3]. Such results suggest that the model system described herein could be used to study the complex relationship among matrix microarchitecture, matrix mechanics, and their associated matrix biochemistry to better understand coordinated physicochemical cell signaling by the extracellular matrix.

5. Conclusions

In this work, the fibrillar microarchitecture of collagen gels was tuned independently of collagen concentration by modulating culture media and gel thickness. Notably, both of these previously underappreciated polymerization parameters induced changes in polymerization kinetics that significantly influenced cell-scale gel structure, as validated by fiber and pore dimensions as well as image autocorrelation methods. To independently probe the influence of gel microarchitecture and bulk density on cell behavior, metastatic MDA-MB-231 cells were embedded within varying collagen I gel structures. Analysis of cell behavior demonstrated that cell-scale gel microarchitecture supercedes bulk matrix density in regulating characteristically invasive behaviors such as bipolar spreading and migration, while gel concentration controls proliferation. These results demonstrate a tractable method for controlling pore size independently of matrix density. Additionally, they highlight the need to monitor gel microarchitecture in common 3D assays of cell behavior where it may be overlooked.

Acknowledgments

This work was supported in part by the Cornell Center on the Microenvironment & Metastasis through Award Number U54CA143876 from the National Cancer Institute to CAR and RMW, National Science Foundation Graduate Research Fellowships to SPC and CMK, and a Howard Hughes Medical Institute Med-Into-Grad Fellowship to SPC.

References

1. Dvorak HF, Weaver VM, Tlsty TD, Bergers G. Tumor microenvironment and progression. J Surg Oncol. 2011; 103:468–74. [PubMed: 21480238]
2. Carey SP, D'Alfonso TM, Shin SJ, Reinhart-King CA. Mechanobiology of tumor invasion: engineering meets oncology. Crit Rev Oncol/Hematol. 201110.1016/j.critrevonc.2011.11.005
3. Provenzano P, Inman D, Eliceiri K, Keely P. Matrix density-induced mechanoregulation of breast cell phenotype, signaling and gene expression through a FAK-ERK linkage. Oncogene. 2009; 28:4326–43. [PubMed: 19826415]
4. Butcher DT, Alliston T, Weaver VM. A tense situation: forcing tumour progression. Nat Rev Cancer. 2009; 9:108–22. [PubMed: 19165226]
5. Ulrich TA, de Juan Pardo EM, Kumar S. The mechanical rigidity of the extracellular matrix regulates the structure, motility, and proliferation of glioma cells. Cancer Res. 2009; 69:4167–74. [PubMed: 19435897]
6. Paszek MJ, Zahir N, Johnson KR, Lakins JN, Rozenberg GI, Gefen A, et al. Tensional homeostasis and the malignant phenotype. Cancer Cell. 2005; 8:241–54. [PubMed: 16169468]
7. Bergamaschi A, Tagliabue E, Sørlie T, Naume B, Triulzi T, Orlandi R, et al. Extracellular matrix signature identifies breast cancer subgroups with different clinical outcome. J Pathol. 2008; 214:357–67. [PubMed: 18044827]
8. Han X, Burke RM, Zettel ML, Tang P, Brown EB. Second harmonic properties of tumor collagen: determining the structural relationship between reactive stroma and healthy stroma. Opt Express. 2008; 16:1846–59. [PubMed: 18542263]
9. Discher DE, Janmey P, Wang Y-L. Tissue cells feel and respond to the stiffness of their substrate. Science. 2005; 310:1139–43. [PubMed: 16293750]
10. Wozniak MA, Chen CS. Mechanotransduction in development: a growing role for contractility. Nat Rev Mol Cell Bio. 2009; 10:34–43. [PubMed: 19197330]
11. Jaalouk DE, Lammerding J. Mechanotransduction gone awry. Nat Rev Mol Cell Bio. 2009; 10:63–73. [PubMed: 19197333]
12. Kraning-Rush C, Califano J, Reinhart-King C. Cellular traction stresses increase with increasing metastatic potential. PloS One. (in press).
13. Pedersen JA, Swartz MA. Mechanobiology in the third dimension. Ann Biomed Eng. 2005; 33:1469–90. [PubMed: 16341917]
14. Friedl P, Wolf K. Plasticity of cell migration: a multiscale tuning model. J Cell Biol. 2010; 188:11–9. [PubMed: 19951899]
15. Pathak A, Kumar S. Biophysical regulation of tumor cell invasion: moving beyond matrix stiffness. Integr Biol. 2011; 3:267–78.
16. Wolf K, Alexander S, Schacht V, Coussens LM, von Andrian UH, van Rheenen J, et al. Collagen-based cell migration models in vitro and in vivo. Semin Cell Dev Biol. 2009; 20:931–41. [PubMed: 19682592]
17. Gelse K. Collagens—structure, function, and biosynthesis. Adv Drug Deliver Rev. 2003; 55:1531–46.
18. Kuntz RM, Saltzman WM. Neutrophil motility in extracellular matrix gels: mesh size and adhesion affect speed of migration. Biophys J. 1997; 72:1472–80. [PubMed: 9138592]
19. Gunzer M, Friedl P, Niggemann B, Brocker E-B, Kampgen E, Zanker KS. Migration of dendritic cells within 3-D collagen lattices is dependent on tissue origin, state of maturation, and matrix structure and is maintained by proinflammatory cytokines. J Leukocyte Biol. 2000; 67:622–9. [PubMed: 10811001]
20. Wolf K, Müller R, Borgmann S, Bröcker E-B, Friedl P. Amoeboid shape change and contact guidance: T-lymphocyte crawling through fibrillar collagen is independent of matrix remodeling by MMPs and other proteases. Blood. 2003; 102:3262–9. [PubMed: 12855577]
21. O'Brien FJ, Harley BA, Yannas IV, Gibson LJ. The effect of pore size on cell adhesion in collagen-GAG scaffolds. Biomaterials. 2005; 26:433–41. [PubMed: 15275817]

22. Provenzano PP, Inman DR, Eliceiri KW, Trier SM, Keely PJ. Contact guidance mediated three-dimensional cell migration is regulated by Rho/ROCK-dependent matrix reorganization. Biophys J. 2008; 95:5374–84. [PubMed: 18775961]
23. Roeder BA, Kokini K, Robinson JP, Voytik-Harbin SL. Local, three-dimensional strain measurements within largely deformed extracellular matrix constructs. J Biomech Eng-T ASME. 2004; 126:699–708.
24. Raub CB, Unruh J, Suresh V, Krasieva T, Lindmo T, Gratton E, et al. Image correlation spectroscopy of multiphoton images correlates with collagen mechanical properties. Biophys J. 2008; 94:2361–73. [PubMed: 18065452]
25. Roeder BA, Kokini K, Voytik-Harbin SL. Fibril microstructure affects strain transmission within collagen extracellular matrices. J Biomech Eng. 2009; 131:031004. [PubMed: 19154063]
26. Raub CB, Suresh V, Krasieva T, Lyubovitsky J, Mih JD, Putnam AJ, et al. Noninvasive assessment of collagen gel microstructure and mechanics using multiphoton microscopy. Biophys J. 2007; 92:2212–22. [PubMed: 17172303]
27. Sander EA, Stylianopoulos T, Tranquillo RT, Barocas VH. Image-based multiscale modeling predicts tissue-level and network-level fiber reorganization in stretched cell-compacted collagen gels. Proc Natl Acad Sci USA. 2009; 106:17675–80. [PubMed: 19805118]
28. Yang YL, Kaufman LJ. Rheology and confocal reflectance microscopy as probes of mechanical properties and structure during collagen and collagen/hyaluronan self-assembly. Biophys J. 2009; 96:1566–85. [PubMed: 19217873]
29. Bailey JL, Critser PJ, Whittington C, Kuske JL, Yoder MC, Voytik-Harbin SL. Collagen oligomers modulate physical and biological properties of three-dimensional self-assembled matrices. Biopolymers. 2011; 95:77–93. [PubMed: 20740490]
30. Van Goethem E, Poincloux R, Gauffre F, Maridonneau-Parini I, Le Cabec V. Matrix architecture dictates three-dimensional migration modes of human macrophages: differential involvement of proteases and podosome-like structures. J Immunol. 2010; 184:1049–61. [PubMed: 20018633]
31. Hakkinen K, Harunaga J, Doyle AD, Yamada KM. Direct comparison of the morphology, migration, cell adhesions, and actin of fibroblasts in four different three-dimensional extracellular matrices. Tissue Eng Part A. 2011; 17:713–24. [PubMed: 20929283]
32. Pizzo AM, Kokini K, Vaughn LC, Waisner BZ, Voytik-Harbin SL. Extracellular matrix (ECM) microstructural composition regulates local cell-ECM biomechanics and fundamental fibroblast behavior: a multidimensional perspective. J Appl Physiol. 2005; 98:1909–21. [PubMed: 15618318]
33. Harjanto D, Maffei JS, Zaman MH. Quantitative analysis of the effect of cancer invasiveness and collagen concentration on 3D matrix remodeling. PloS one. 2011; 6:e24891. [PubMed: 21980363]
34. Zaman MH, Trapani LM, Sieminski AL, MacKellar D, Gong H, Kamm RD, et al. Migration of tumor cells in 3D matrices is governed by matrix stiffness along with cell-matrix adhesion and proteolysis. Proc Natl Acad Sci USA. 2006; 103:10889–94. [PubMed: 16832052]
35. Miron-Mendoza M, Seemann J, Grinnell F. The differential regulation of cell motile activity through matrix stiffness and porosity in three dimensional collagen matrices. Biomaterials. 2010; 31:6425–35. [PubMed: 20537378]
36. Baker EL, Srivastava J, Yu D, Bonnecaze RT, Zaman MH. Cancer cell migration: integrated roles of matrix mechanics and transforming potential. PloS One. 2011; 6:e20355. [PubMed: 21647371]
37. Yang YL, Sun C, Wilhelm ME, Fox LJ, Zhu J, Kaufman LJ. Influence of chondroitin sulfate and hyaluronic acid on structure, mechanical properties, and glioma invasion of collagen I gels. Biomaterials. 2011; 32:7932–40. [PubMed: 21820735]
38. Ulrich TA, Jain A, Tanner K, MacKay JL, Kumar S. Probing cellular mechanobiology in three-dimensional culture with collagen-agarose matrices. Biomaterials. 2010; 31:1875–84. [PubMed: 19926126]
39. Gobeaux F, Mosser G, Anglo A, Panine P, Davidson P, Giraud-Guille M, et al. Fibrillogenesis in dense collagen solutions: a physicochemical study. J Mol Biol. 2008; 376:1509–22. [PubMed: 18234220]
40. Yang YL, Motte S, Kaufman LJ. Pore size variable type I collagen gels and their interaction with glioma cells. Biomaterials. 2010; 31:5678–88. [PubMed: 20430434]

41. Williams RM, Ellenson LH, Connolly DC, Hamilton TC, Nikitin AY, Zipfel WR. Strategies for high-resolution imaging of epithelial ovarian cancer by laparoscopic nonlinear microscopy. Transl Oncol. 2010; 3:181–94. [PubMed: 20563260]
42. Petersen NO, Höddelius PL, Wiseman PW, Seger O, Magnusson KE. Quantitation of membrane receptor distributions by image correlation spectroscopy: concept and application. Biophys J. 1993; 65:1135–46. [PubMed: 8241393]
43. Provenzano PP, Inman DR, Eliceiri KW, Knittel JG, Yan L, Rueden CT, et al. Collagen density promotes mammary tumor initiation and progression. BMC Med. 2008:6. [PubMed: 18279502]
44. Provenzano PP, Eliceiri KW, Campbell JM, Inman DR, White JG, Keely PJ. Collagen reorganization at the tumor-stromal interface facilitates local invasion. BMC Med. 2006:4. [PubMed: 16515705]
45. Levental KR, Yu H, Kass L, Lakins JN, Egeblad M, Erler JT, et al. Matrix crosslinking forces tumor progression by enhancing integrin signaling. Cell. 2009; 139:891–906. [PubMed: 19931152]
46. Wolf K, Wu YI, Liu Y, Geiger J, Tam E, Overall C, et al. Multi-step pericellular proteolysis controls the transition from individual to collective cancer cell invasion. Nat Cell Biol. 2007; 9:893–904. [PubMed: 17618273]
47. Yamada KM, Cukierman E. Modeling tissue morphogenesis and cancer in 3D. Cell. 2007; 130:601–10. [PubMed: 17719539]
48. Kraning-Rush CM, Carey SP, Califano JP, Smith BN, Reinhart-King CA. The role of the cytoskeleton in cellular force generation in 2D and 3D environments. Phys Biol. 2011; 8:015009. [PubMed: 21301071]
49. Petrie RJ, Doyle AD, Yamada KM. Random versus directionally persistent cell migration. Nat Rev Mol Cell Bio. 2009; 10:538–49. [PubMed: 19603038]
50. Olson MF, Sahai E. The actin cytoskeleton in cancer cell motility. Clin Exp Metastasis. 2009; 26:273–87. [PubMed: 18498004]
51. Carey, SP.; Charest, JM.; Reinhart-King, CA. Forces during cell adhesion and spreading: implications for cellular homeostasis. In: Gefen, A., editor. Cellular and Biomolecular Mechanics and Mechanobiology. Berlin and Heidelberg: Springer-Verlag; 2011. p. 29-69.
52. Friedl P, Wolf K, Lammerding J. Nuclear mechanics during cell migration. Curr Opin Cell Biol. 2011; 23:55–64. [PubMed: 21109415]
53. Fraley SI, Feng Y, Krishnamurthy R, Kim D, Celedon A, Longmore GD, et al. A distinctive role for focal adhesion proteins in three-dimensional cell motility. Nat Cell Biol. 2010; 12:598–604. [PubMed: 20473295]
54. Hotary KB, Allen ED, Brooks PC, Datta NS, Long MW, Weiss SJ. Membrane type I matrix metalloproteinase usurps tumor growth control imposed by the three-dimensional extracellular matrix. Cell. 2003; 114:33–45. [PubMed: 12859896]

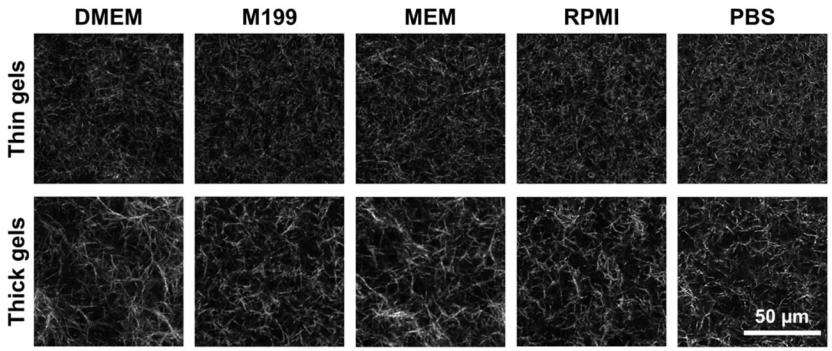

Figure 1.

Confocal reflectance microscopy reveals differential collagen gel microarchitectures in response to media formulation and gel thickness. Confocal reflectance images (40×, 2× zoom) of 1.5 mg/mL collagen gels made with different media formulations and in two thicknesses. All gels were polymerized at 37°C in a glass-bottom 24-well plate. “Thin gels” (top) were made with 250 μL of gel solution and were ~1.5 mm thick; “thick gels” (bottom) were made with 1000 μL of gel solution and were ~5.3 mm thick. Each image is a 1-μm thick slice taken 200 μm into collagen gel. Scale bar = 50 μm.

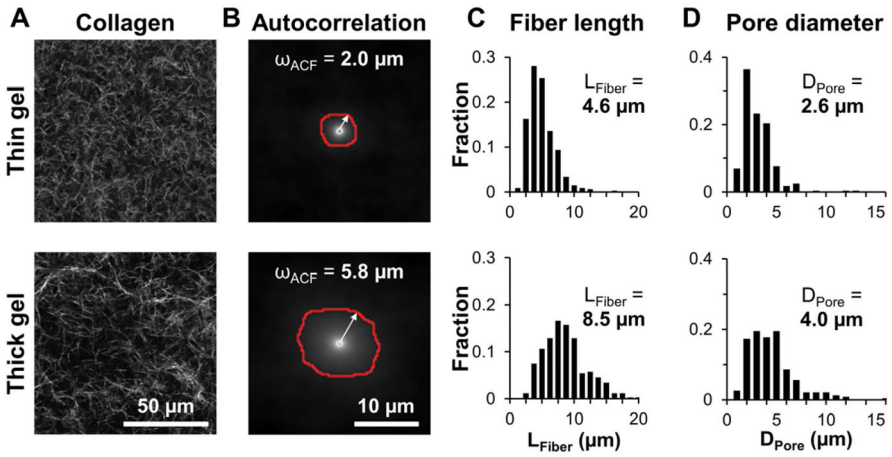

Figure 2.

Quantitative analysis of collagen gel microarchitecture with image autocorrelation analysis. (A) Representative confocal reflectance images of thin (top) and thick (bottom) collagen gels made with MEM. (B) Autocorrelation functions of the confocal reflectance images in (A). Red outlines represent the $1/e^2$ radii, or ω_{ACF} characteristic lengths, whose means were 2.0 μm and 5.8 μm for the thin and thick gels, respectively. (C) Distributions of collagen fiber lengths in (A), whose means were 4.6 μm and 8.5 μm for the thin and thick gels, respectively (>300 fibers measured per image). **(D)** Distributions of pore diameters in (A), whose means were 2.6 μm and 4.0 μm for the thin and thick gels, respectively (>200 pores measured per image).

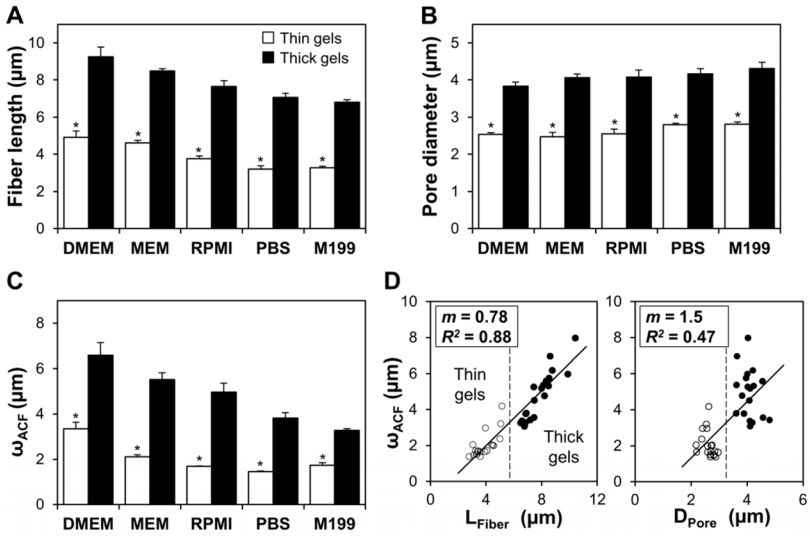

Figure 3.

Collagen gel microarchitectural features are sensitive to media formulation and gel thickness. (A) Mean collagen fiber lengths and (B) pore diameters for thin (open bars) and thick (filled bars) collagen gels made with different media formulations. (C) Mean ω_{ACF} characteristic lengths ($1/e^2$ radii from autocorrelation function) for thin (open bars) and thick (filled bars) collagen gels made with different media formulations. For (A)-(C), n = 4 images from two gels per condition; * indicates statistically significant difference between thin and thick media-matched gels. (D) Comparison of each image's mean fiber length (L_{Fiber}, left) and mean pore diameter (D_{pore}, right) with its mean ω_{ACF} characteristic length; dashed vertical lines graphically differentiate thin gels (open circles) from thick gels (filled circles); slopes and R^2 values for best-fit lines are given in the figure.

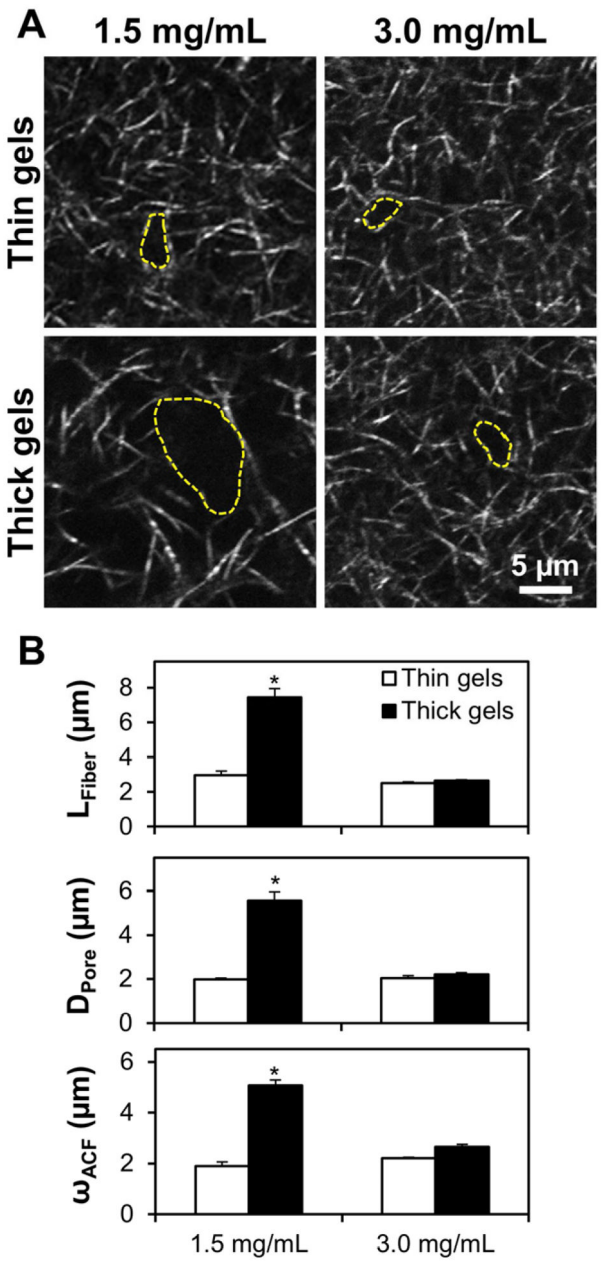

Figure 4.

Collagen gels for cell behavior studies. (A) High-power (40×, 3× zoom) confocal reflectance images of 1.5 mg/mL (left) and 3.0 mg/mL (right) collagen gels polymerized in thin (top) and thick (bottom) volumes. Representative pores are highlighted (dashed yellow line). (B) Microarchitectural features were calculated as previously shown for thin (open bars) and thick (filled bars) gels; n = 4 images from two gels per condition; * indicates statistically significant difference between thick 1.5 mg/mL gels and all other conditions. Scale bar = 5 μm.

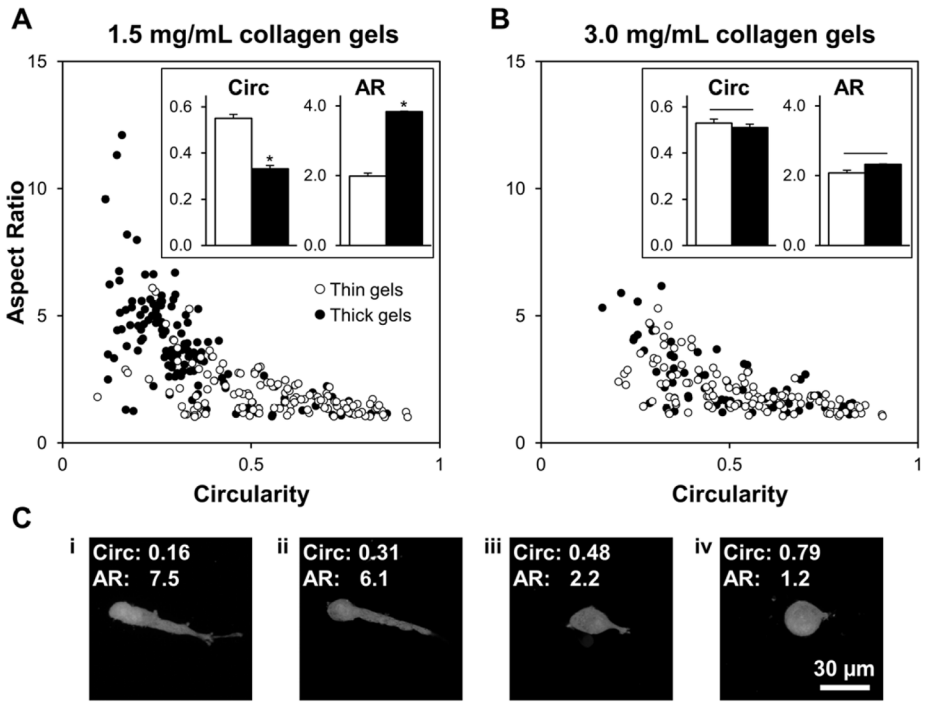

Figure 5.

Collagen gel microarchitecture impacts cell morphology. Morphologies of MDA-MB-231/GFP cells were determined by analyzing the circularity (x-axis) and aspect ratio (y-axis) of cells embedded in (A) 1.5 mg/mL and (B) 3.0 mg/mL gels; each data point represents a single cell. Circularity (4π x area/perimeter^2) describes the roundness of a cell and can range from 0 to 1, with 1 denoting circular cells; aspect ratio (major axis/minor axis) describes the elongation of a cell and is larger than 1, with increasing values denoting increasingly polarized morphology. *Insets:* Mean morphological parameters for each concentration and gel thickness condition; n ≥ 75 cells per condition from three independent experiments; * indicates statistically significant difference between thick 1.5 mg/mL gels and all other conditions. (C) Representative z-projected images of embedded MDA-MB-231/GFP cells demonstrate bipolar (i-ii) and rounded (iii-iv) morphologies. Scale bar = 30 μm.

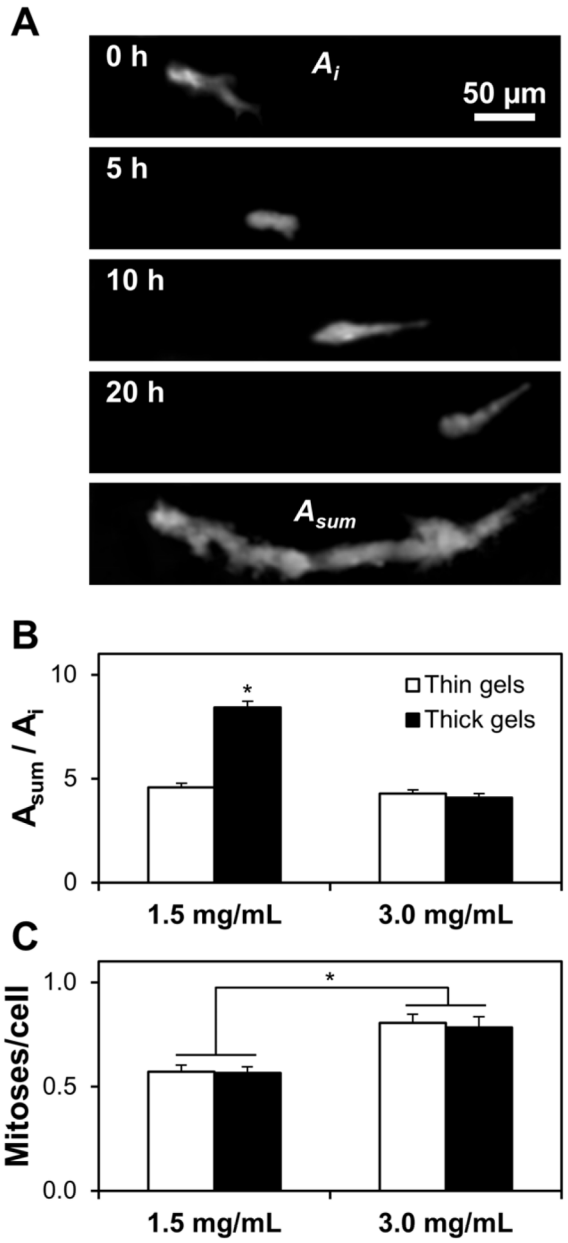

Figure 6.

Collagen gel microarchitecture impacts cell migration while bulk gel concentration impacts cell proliferation. (A) Representative time-series of a MDA-MB-231/GFP cell migrating through a thick 1.5 mg/mL 3D collagen gel. Time points (0 h – 20 h) are projections of confocal z-stacks; the final panel is the time-projection of all z-stacks, representing the migration history of the cell (A_{sum}). (B) Migration index was calculated as the ratio of a cell's time-projected area to its initial area (A_{sum}/A_i) for cells randomly migrating within thin (open bars) and thick (filled bars) 1.5 mg/mL and 3.0 mg/mL gels; n ≥ 30 cells per condition; * indicates statistically significant difference between thick 1.5 mg/mL gels and all other conditions. (C) Cell proliferation was assessed from time-lapse videos of cells embedded within thin (open bars) and thick (filled bars) 1.5 mg/mL and 3.0 mg/mL gels; n ≥ 15 fields of view per condition; * indicates statistically significant difference between 1.5

mg/mL and 3.0 mg/mL collagen gels; no difference was observed between thick and thin gels of the same collagen density. Scale bar = 50 μm.